Spin-Crossover Nanoparticles

DOI: 10.1002/anie.201301562

Photoinduced Relaxation Dynamics in Iron(II) Spin-Crossover Nanoparticles: The Significance of Crystallinity**

Pradip Chakraborty, Marie-Laure Boillot, Antoine Tissot, and Andreas Hauser**

Switchable molecular materials are of interest for future applications because their physical properties can be tuned by various external stimuli.[1] Among these, electromagnetic radiation is a convenient tool for controlling functionalities such as magnetic, optical, structural, and electrical properties. Spin-crossover compounds are prototypes of switchable solids, as their spin state can be switched from low-spin (LS) to high-spin (HS) as a function of temperature, pressure, and light.[2,3] Potential applications in information technology and memory devices require processing of such materials in the form of nano-objects. Thus, a lot of work has been dedicated to study size-reduction effects on the switching behavior of spin-crossover solids,[4] mostly focusing on the influence of particle size on cooperative effects during the thermal spin transition using 1D and 3D coordination polymers.[5] In contrast, the photoinduced spin switching dynamics of spin-crossover nanoparticles as well as the synthesis of spin-crossover nano-objects built with complexes of molecular nature remain almost unexplored.

Recently, the synthesis of amorphous spin-crossover nanoparticles of $[Fe(mepy)_3tren](PF_6)_2$, $(mepy)_3tren$ = tris{4-[(6-methyl)-2-pyridyl]-3-aza-3-butenyl}amine, as well as preliminary results on their photoswitching behavior based on light-induced excited spin state trapping (LIESST) have been described,[6] and Neville et al. reported the preparation of photoswitchable nano-objects of a 2D coordination polymer.[7] The photoswitching process, probed by ultrafast optical spectroscopy, may also be affected by size reduction.[8] However, the relationship between particle size and the properties of the metastable HS state has not been established yet.

Herein we report the application of the recently elaborated method based on fast precipitation in an anti-solvent[9] for the preparation of $[Fe(mepy)_3tren](PF_6)_2$ nanocrystals and present a detailed study of their photoinduced HS→LS relaxation behavior. Furthermore, the behavior of the nanocrystals is compared with that of the previously reported 50 nm amorphous particles of the same compound.

The TEM image of a dispersion of the precipitated nanoparticles of $[Fe(mepy)_3tren](PF_6)_2$ in EtOH shows well-dispersed spherical nanoparticles with an average size of (74 ± 10) nm and a satisfactorily narrow size distribution (Figure 1 a,b). The powder X-ray diffraction pattern of the nanoparticles shows peaks at the same positions and the same intensities as polycrystalline $[Fe(mepy)_3tren](PF_6)_2$, indicating that the nanoparticles are indeed crystalline and belong to the same space group as the bulk material (Figure 1 c).

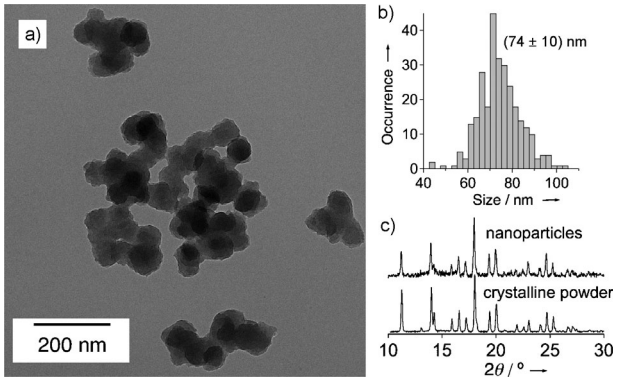

Figure 1. TEM image (a) and size distribution (b) of crystalline $[Fe(mepy)_3tren](PF_6)_2$ nanoparticles. Powder X-ray diffraction patterns of the nanoparticles and polycrystalline powder (c).

Figure 2 illustrates the thermal spin-crossover behavior of the crystalline nanoparticles and the reference polycrystalline compound determined by magnetic susceptibility measurements (Figure S1, see the Supporting Information) and optical absorption spectroscopy. The magnetic measurements show that the thermal spin transition of the crystalline nanoparticles is fairly steep and occurs at a transition temperature of $T_{1/2} = 215$ K. It has a more gradual low-temperature tail with a residual HS fraction, γ_{HS}, of about 17%. In comparison, the thermal transition for the polycrystalline reference compound is complete, somewhat steeper and occurs at almost the same temperature.[10] Temperature-dependent variations of the spin-allowed metal–ligand charge transfer (^{1}MLCT) absorption band in the visible region ($\lambda_{max} \approx 580$ nm) are observed during the spin transition (Figure 2, inset) for crystalline nanoparticles dispersed in Nujol. The evolution of γ_{HS} can thus be monitored by optical spectroscopy, by following the intensity of the ^{1}MLCT as a function of temperature after normalization with the data from the magnetic measurements (see Figure S2 in the

[*] Dr. P. Chakraborty, Dr. A. Tissot, Prof. A. Hauser
Département de Chimie Physique, Université de Genève
30, quai Ernest Ansermet, 1211 Genève (Switzerland)
E-mail: antoine.tissot@unige.ch
andreas.hauser@unige.ch
Dr. M.-L. Boillot
ICMMO-ECI, UMR CNRS 8182, Université Paris-Sud
15 Rue G. Clemenceau, 91405 Orsay (France)

[**] This work was supported by the Swiss National Science Foundation (Grant No. 200020_137567). N. Amstutz is thanked for the synthesis of the starting compounds and C. Enachescu for his help in data modeling.

Supporting information for this article is available on the WWW under http://dx.doi.org/10.1002/anie.201301562.

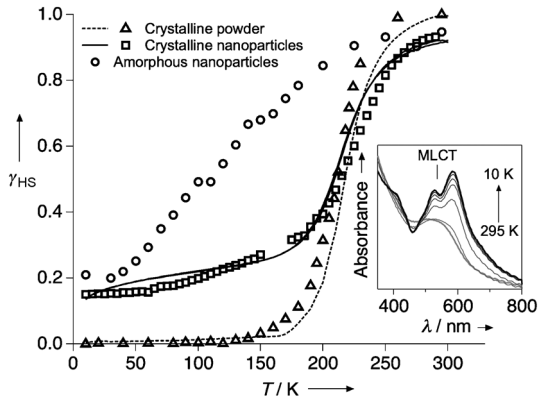

Figure 2. Thermal spin-transition curves for crystalline nanoparticles, amorphous nanoparticles (adapted from Ref. [6]) and the reference crystalline powder of $[Fe(mepy)_3tren](PF_6)_2$ taken from magnetic susceptibility measurements (——, – – –) and optical spectroscopy (○, △, □). Inset: variable-temperature optical absorption spectra of crystalline nanoparticles dispersed in Nujol.

Supporting Information for the analysis on single-crystal optical data). Both methods give comparable results, with a thermal spin transition centered at $T_{1/2} = 215$ K. For comparison, Figure 2 also includes the spin-transition curve obtained by optical spectroscopy of amorphous nanoparticles. It is much more gradual than for the polycrystalline reference compound as well as for the crystalline nanoparticles and with $T_{1/2} = 125$ K it is shifted towards lower temperature. Similar to the crystalline nanoparticles, the amorphous nanoparticles also exhibit a residual HS fraction of approximately 20% at low temperature.

For coordination-network-based spin-crossover nanoparticles such a temperature shift and a residual HS fraction are usually attributed to the size-reduction effect, as for such objects the coordination sphere of the Fe centers located at the surface can be incomplete.[4,5] However, the residual HS fraction can also be due to core defects rather than to surface effects, as in the present case the nanoparticles are made of complexes of a molecular nature and have therefore the same coordination sphere at the surface and in the core.[9] The difference observed between crystalline and amorphous particles of similar size in fact demonstrates the influence of disorder versus crystallinity on the thermal spin-crossover behavior. In the amorphous nano-objects, with the spin-transition temperature at lower temperature, the HS state is stabilized because of the less-dense arrangement of spin-crossover molecules in the amorphous solid compared to the crystalline one.

Photoinduced HS→LS relaxation based on the LIESST effect was probed on crystalline nanoparticles by means of optical spectroscopy. Photoexcitation was carried out at 532 nm, which corresponds to the ^{1}MLCT absorption band of the complex. Even at the lowest temperature of 4 K the relaxation occurs on a timescale of a few seconds. In a first step, the laser power was optimized at 4 K to achieve a quantitative photoinduced conversion and to minimize laser-induced heating of the sample. Photoexcitation curves at 4 K are close to single exponential (Figure S3) and can be analyzed using Equation (1), which expresses the competition between excitation and relaxation, where k_{HL} is the HS→LS relaxation rate constant and k_{ex} the excitation rate constant.

$$\frac{d\gamma_{HS}}{dt} = k_{ex}(1-\gamma_{HS}) - k_{HL}\gamma_{HS} \quad (1)$$

Figure 3 shows the evolution of the photoexcitation rate constant k_{ex} and of the steady-state value of the HS fraction reached under continuous irradiation, γ_{HS}^{ss}, with laser power.

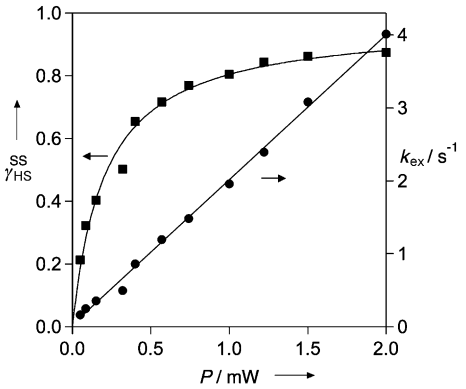

Figure 3. Analysis of the photoexcitation measurements performed at 4 K on crystalline $[Fe(mepy)_3tren](PF_6)_2$ nanoparticles dispersed in Nujol: (●) excitation rate constant k_{ex} versus laser power; (■) steady-state HS fraction γ_{HS}^{ss} versus laser power (2 mW correspond to ca. 1 mW mm^{-2}).

k_{ex} increases linearly with the laser power, as expected for homogeneous photoexcitation with a sample where the optical density (OD) at 532 nm is less than 0.3 and therefore no concentration gradients occurs. γ_{HS}^{ss} also depends on the laser power and can be fitted with Equation (2) (see the

$$\gamma_{HS}^{SS} = \frac{k_{ex}}{k_{ex}+k_{HL}} = \frac{1}{1+c/P} \quad (2)$$

Supporting Information for details) where c is a scaling constant and P the laser power.

Thus, at a laser power of 2 mW, a steady-state HS fraction of 85% can be achieved.

Relaxation curves after switching off the laser are close to single exponential in nature, with a rate constant that is almost laser-power independent (Figure S4 and S5), however with small but systematic deviations from single exponential. These deviations are not consistent with cooperative effects because the relaxation is faster at the beginning and slower towards the end compared to the single-exponential fit. They are not due to laser-induced heating either, as the relative deviations are laser-power independent. Therefore, even in crystalline nanoparticles, they are probably due to an inhomogeneous distribution of environments that may arise from sites located at the surface of the particles.

Figure 4a shows the temperature dependence of the HS→LS relaxation curves for crystalline nanoparticles. As mentioned above, the relaxation process is close to single

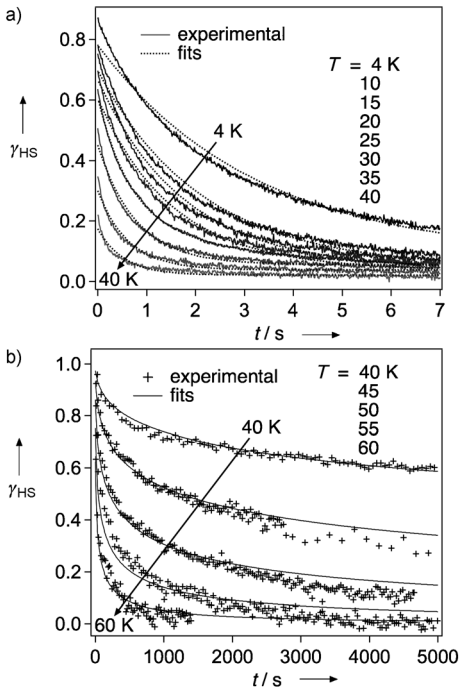

Figure 4. Variable temperature HS→LS relaxation curves obtained after photoexcitation at 532 nm for a) the crystalline particles from the photostationary state and single exponential fits, and b) the amorphous particles from quantitative excitation along with their single exponential model curves, taking into account an inhomogeneous distribution of environments with $E_a = 550\ cm^{-1}$ and $\sigma(E_a) = 100\ cm^{-1}$. Note the timescale difference between (a) and (b).

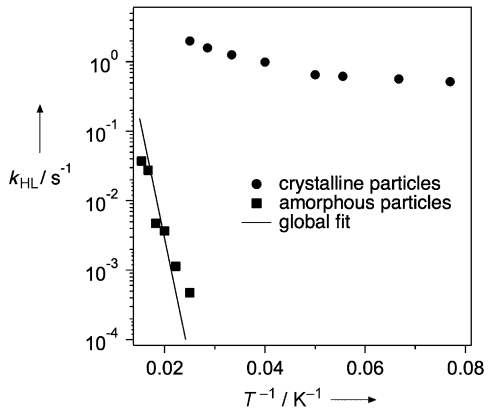

Figure 5. Arrhenius plot of the average HS→LS relaxation rate constant for crystalline (●) and amorphous (■) $[Fe(mepy)_3tren](PF_6)_2$ nanoparticles, along with the values obtained with the global fit on the amorphous particles (——).

exponential, with a HS state lifetime of approximately 2 s at 4 K and 0.5 s at 40 K. For comparison, Figure 4b shows HS→LS relaxation curves for the amorphous particles trapped in transparent silica films.[6] They are very different in shape, having the form of stretched exponentials. With a value on the order of 10^4 s at 40 K, the lifetime of the photoinduced HS state is also several orders of magnitude longer than for the crystalline nanoparticles. Ignoring the small deviations from single exponential decay for the crystalline nanoparticles, an approximate value for k_{HL} as a function of temperature can be obtained by exponential fits. For the amorphous nanoparticles the stretched exponential curves are attributed to a large inhomogeneous distribution of the zero-point energy difference between the two spin manifolds. This situation can be accounted for by a Gaussian distribution of activation energies around an average value.[11] A global fit satisfactorily reproduces the experimental relaxation curves in the temperature interval of the experiment with an apparent activation energy $E_a = 550\ cm^{-1}$, a pre-exponential factor $A = 2.5 \times 10^4\ s^{-1}$ and a standard deviation of $\sigma(E_a) = 100\ cm^{-1}$. The large distribution of activation energies confirms the large distribution of environments in the amorphous nanoparticles. The fit value of E_a is coherent with previous results on doped $[Zn_{1-x}Fe_x(mepy)_3tren](PF_6)_2$ single crystals.[12]

As an alternative, average relaxation rate constants can be extracted from the stretched exponentials according to a published procedure.[13] Figure 5 shows the average values of k_{HL} for the crystalline and amorphous nanoparticles plotted on a logarithmic scale versus T^{-1} (Arrhenius plot). For both samples, the relaxation rate constant is strongly temperature dependent above 30 K, which is characteristic of a thermally activated relaxation process. Below 30 K, the relaxation of the crystalline particles is almost temperature independent, which is consistent with a relaxation process governed by quantum-mechanical tunneling by a non-adiabatic multiphonon type process.[14]

In addition to the different shapes of the relaxation curves, an important feature is the difference in the timescales between the two samples, estimated to be around five orders of magnitude at 40 K. This observation can be related to the above-mentioned difference in thermal transition temperature between the two different kinds of nanoparticles, that is, 125 K for the amorphous and 215 K for the crystalline nano-objects. Indeed, the relaxation rate constant in the tunneling regime varies exponentially with the thermal spin-transition temperature, with expected values of 10^{-2}–$1\ s^{-1}$ for $T_{1/2} = 215$ K and 10^{-4}–$10^{-6}\ s^{-1}$ for $T_{1/2} = 125$ K.[3] They are thus fully consistent with the relaxation timescales observed for the amorphous and crystalline nanoparticles.

In conclusion, we report the synthesis of (74 ± 10) nm spin-crossover nanocrystals based on the molecular spin-crossover compound $[Fe(mepy)_3tren](PF_6)_2$. The thermal spin transition of these objects, centered at 215 K, has been investigated by both magnetic and optical methods, showing a slightly more gradual thermal conversion than their bulk reference compound. The photoswitching behavior of the crystalline nano-objects has been investigated by optical spectroscopy and compared to that of amorphous objects of the same composition and similar size, the amorphous objects exhibit a very gradual spin transition centered at 125 K. The HS→LS relaxation kinetics are significantly different in terms of timescale, that is, 10^{-1} s versus 10^4 s at 40 K, and shape, that is, single exponential versus stretched exponential, between crystalline and amorphous particles, respectively. These observations are attributed to the difference in crystallinity between the samples. Amorphous particles have a lower transition temperature because of the less-dense packing. This arrangement results in slower relaxation kinetics than in

the crystalline particles. This effect is of interest not only for specialists working in the area of spin-crossover, but to physicists and chemists interested in nanomaterials and photoinduced phenomena in general. As in even-smaller particles the surface-to-volume ratio is expected to play an even more important role in the dynamics of photoexcitation and relaxation, the synthesis of size-controlled smaller crystalline particles is now underway. As a further tool, ultrafast spectroscopy will give additional insight into the actual switching mechanism in nanocrystals, in particular with regard to the different timescales involved in the switching process.[15]

Experimental Section

The synthesis and characterization of amorphous in-silica nanoparticles of $[Fe(mepy)_3tren](PF_6)_2$ were described elsewhere.[6] $[Fe(mepy)_3tren](PF_6)_2$ and $[Fe(mepy)_3tren]Cl_2$ in the form of crystalline powder, were prepared following the strategy described in the literature.[10] The $[Fe(mepy)_3tren]Cl_2$ was used as starting material for the synthesis of crystalline nanoparticles. The products were characterized by infrared spectroscopy and typical absorption peaks, characteristic of the HS $[Fe(mepy)_3tren](PF_6)_2$ complex, were found (see Figure S6). For the preparation of crystalline nanoparticles $[Fe(mepy)_3tren]Cl_2$ (0.1 mmol, 58.2 mg) dissolved in MeOH (4 mL) were added dropwise to $NaPF_6$ (2 mmol, 336 mg) dissolved in MeOH (6 mL) under vigorous stirring. A red precipitate was observed within a few seconds. After 15 min, the precipitate was collected by centrifugation, washed two times with EtOH and finally dried under vacuum.

The powder collected after centrifugation was dispersed in pentane and few drops of the dispersion were drop casted on a carbon-coated copper grid (Formar Carbon film, 200 Mesh). TEM images were taken with a FEI Tecnai G2 Sphera with 100 keV electrons focused on the sample.

Powder X-Ray diffraction (XRD) was performed with a Bruker D8 Advance diffractometer equipped with a $Cu_{K\alpha}$ X-Ray source in a Bragg–Brentano geometry. Patterns were registered between 5 and 40° with 6 h integration time.

For optical measurements, nanoparticles were dispersed in Nujol oil. The dispersion was placed between two sapphire disks in a home-built sample holder and cooled down with a closed cycle He cryostat capable of achieving temperatures down to 4 K (Janis-Sumitomo SHI-4.5) and equipped with a programmable temperature controller (LakeShore Model 331). High-quality absorption spectra were recorded on a double beam spectrometer (Varian Cary 5000). Photoexcitation was carried out with a cw diode pumped solid-state laser at 532 nm (ILEE VA-I-N-532). The maximum Laser power used, that is, 2 mW, corresponds to approximately 1 $mW\,mm^{-2}$, which leads to a steady-state after about 1 s at 4 K, owing to the high absorption of the LS sample at 532 nm ($\varepsilon \approx 5000\,M^{-1}cm^{-1}$). The HS→LS relaxation was probed with different techniques depending on the lifetime of the metastable HS state. For the amorphous particles, where the relaxation is slow enough, the temporal evolution of the absorption spectrum was monitored using a home-built system with a Xenon lamp (Osram XBO) and a single monochromator (Spex 270M) coupled to a CCD camera (Jobin–Yvon CCD 3500). For the crystalline particles, a similar setup was used but with a single wavelength probe at 570 nm, using a photomultiplier (Hamamatsu R928) and a photon-counting system (Stanford Research SR400).

Received: February 22, 2013
Published online: June 5, 2013

Keywords: crystallinity · nanoparticles · optical spectroscopy · spin crossover · spin relaxation

[1] a) *Molecular Switches, 2nd ed.* (Ed.: B. Feringa), Wiley-VCH, Weinheim, **2001**; b) O. Sato, J. Tao, Y.-Z. Zhang, *Angew. Chem.* **2007**, *119*, 2200; *Angew. Chem. Int. Ed.* **2007**, *46*, 2152.
[2] a) P. Gütlich, A. Hauser, H. Spiering, *Angew. Chem.* **1994**, *106*, 2109; *Angew. Chem. Int. Ed. Engl.* **1994**, *33*, 2024; b) "Spin-Crossover in Transition Metal Compounds, I–III": *Top. Curr. Chem. 233–235* (Eds.: P. Gütlich, H. A. Goodwin), Springer, Berlin, **2004**.
[3] A. Hauser, *Top. Curr. Chem.* **2004**, *234*, 155.
[4] A. Bousseksou, G. Molnar, L. Salmon, W. Nicolazzi, *Chem. Soc. Rev.* **2011**, *40*, 3313; H. J. Shepherd, G. Molnár, W. Nicolazzi, L. Salmon, A. Bousseksou, *Eur. J. Inorg. Chem.* **2013**, 653.
[5] a) E. Coronado, J. R. Galán-Mascarós, M. Monrabal-Capilla, J. García-Martínez, P. Pardo-Ibáñez, *Adv. Mater.* **2007**, *19*, 1359; b) T. Forestier, A. Kaiba, S. Pechev, D. Denux, P. Guionneau, C. Etrillard, N. Daro, E. Freysz, J.-F. Létard, *Chem. Eur. J.* **2009**, *15*, 6122; c) A. Tokarev, L. Salmon, Y. Guari, W. Nicolazzi, G. Molnar, A. Bousseksou, *Chem. Commun.* **2010**, *46*, 8011; d) I. Boldog, A. B. Gaspar, V. Martinez, P. Pardo-Ibáñez, V. Ksenofontov, A. Bhattacharjee, P. Gütlich, J. A. Real, *Angew. Chem.* **2008**, *120*, 6533; *Angew. Chem. Int. Ed.* **2008**, *47*, 6433; e) J. Larionova, L. Salmon, Y. Guari, A. Tokarev, K. Molvinger, G. Molnar, A. Bousseksou, *Angew. Chem.* **2008**, *120*, 8360; *Angew. Chem. Int. Ed.* **2008**, *47*, 8236; f) F. Volatron, L. Catala, E. Rivière, A. Gloter, O. Stéphan, T. Mallah, *Inorg. Chem.* **2008**, *47*, 6584.
[6] A. Tissot, J.-F. Bardeau, E. Rivière, F. Brisset, M.-L. Boillot, *Dalton Trans.* **2010**, *39*, 7806.
[7] S. M. Neville, C. Etrillard, S. Asthana, J.-F. Létard, *Eur. J. Inorg. Chem.* **2010**, 282.
[8] R. Bertoni, M. Lorenc, A. Tissot, M. Servol, M.-L. Boillot, E. Collet, *Angew. Chem.* **2012**, *124*, 7603; *Angew. Chem. Int. Ed.* **2012**, *51*, 7485.
[9] A. Tissot, L. Rechignat, A. Bousseksou, M.-L. Boillot, *J. Mater. Chem.* **2012**, *22*, 3411.
[10] M. A. Hoselton, L. J. Wilson, R. S. Drago, *J. Am. Chem. Soc.* **1975**, *97*, 1722.
[11] A. Hauser, J. Adler, P. Gütlich, *Chem. Phys. Lett.* **1988**, *152*, 468.
[12] A. Hauser, A. Vef, P. Adler, *J. Chem. Phys.* **1991**, *95*, 8710.
[13] C. Enachescu, A. Hauser, J.-J. Girerd, M.-L. Boillot, *ChemPhysChem* **2006**, *7*, 1127.
[14] E. Buhks, G. Navon, M. Bixon, J. Jortner, *J. Am. Chem. Soc.* **1980**, *102*, 2918.
[15] M. Lorenc, C. Baldé, W. Kaszub, A. Tissot, N. Moisan, M. Servol, M. Buron-Le Cointe, H. Cailleau, P. Chasle, P. Czarnecki, M. L. Boillot, E. Collet, *Phys. Rev. B* **2012**, *85*, 054302.

